Anderson Localization of Ultracold Atoms: Where is the Mobility Edge?

Michael Pasek,[1,2,3,*] Giuliano Orso,[1] and Dominique Delande[2]
[1]Laboratoire Matériaux et Phénomènes Quantiques, Université Paris Diderot-Paris 7 and CNRS, UMR 7162, 75205 Paris Cedex 13, France
[2]Laboratoire Kastler Brossel, UPMC-Sorbonne Universités, CNRS, ENS-PSL Research University, Collège de France, 4 Place Jussieu, 75005 Paris, France
[3]Laboratoire Charles Fabry de l'Institut d'Optique, Centre National de la Recherche Scientifique et Université Paris Sud 11, Bât. 503, Campus Universitaire d'Orsay, 91403 Orsay Cedex, France
(Received 15 November 2016; revised manuscript received 10 February 2017; published 28 April 2017)

Recent experiments in noninteracting ultracold atoms in three-dimensional speckle potentials have yielded conflicting results regarding the so-called mobility edge, i.e., the energy threshold separating Anderson localized from diffusive states. At the same time, there are theoretical indications that most experimental data overestimate this critical energy, sometimes by a large amount. Using extensive numerical simulations, we show that the effect of anisotropy in the spatial correlations of realistic disorder configurations alone is not sufficient to explain the experimental data. In particular, we find that the mobility edge obeys a universal scaling behavior, independently of the speckle geometry.

DOI: 10.1103/PhysRevLett.118.170403

When a wave travels in a random medium, the interference between multiple scattering paths caused by the disorder barriers can completely stop its diffusion. This phenomenon, known as Anderson localization [1], is completely general and applies to any kind of waves including light waves in diffusive media [2,3] or in photonic crystals [4,5], ultrasound [6], microwaves [7], and atomic matter waves [8,9]. Localization experiments using noninteracting cold atomic gases have several advantages over their solid-state counterparts [10,11]. The inhibition of transport is directly measured by probing the expansion of a wave packet in the presence of disorder. The effect of interactions, which unavoidably hinders localization measurements in solid-state systems, can here be reduced by diluting the Bose-Einstein condensate or by using Feshbach resonances. Last, far-detuned laser speckles can be used as tunable disordered potentials, allowing the exploration of the localization phase diagram.

Several experiments [12–14] on cold atomic gases have attempted to characterize metal-insulator Anderson transitions in three dimensions, starting from a precise measurement of the mobility edge. This turns out to be difficult, both theoretically and experimentally. Since the Anderson transition is a second-order quantum phase transition [15], the localization length diverges on the localized side and the diffusion coefficient slowly vanishes on the diffusive side. Distinguishing the two behaviors requires long observation times [16], which is not easily achievable in experiments. Moreover, an atomic wave packet expanding in a random potential inevitably contains states at different energies, thus mixing localized and extended components. For these reasons, results on the position of the mobility edge are widely spread. On the theoretical side, the metal-insulator transition takes place in the strongly scattering regime where perturbative expansions fail. For spatially correlated disorder, there is no reliable analytical method predicting accurately the position of the mobility edge [17–20] and one has to resort to the indignity of numerical calculations. The first quasi-exact numerical estimations [17,21] of the mobility edge lie significantly below most experimental measurements. It has been proposed [14] that the anisotropic correlation functions of realistic disordered potentials, not taken into account in Ref. [17], could be at the origin of this discrepancy. Reproducing all minute details of experimental speckle configurations in numerical simulations is cumbersome, if desirable at all. It would be more profitable to understand how the mobility edge changes with speckle geometry, and know its more universal features. In the present Letter, we show that there exists a *nontrivial* scaling of the mobility edge, given in Eq. (4) below, involving a renormalization of the amplitude of the disordered potential. This allows us to take into account the effect of anisotropy on the localization phase diagram by a proper rescaling of the characteristic energies. This crucial point was overlooked in a previous numerical study [21], because the anisotropy was varied at constant disorder strength, while the proper scaling variable is the ratio of the disorder strength to the anisotropy-dependent correlation energy.

Disordered optical potentials used in current experiments are created by shining coherent laser beams through diffusive plates, as sketched in Fig. 1(a). The shift of atomic energy levels due to light-matter coupling is proportional to the intensity of radiation I, yielding an effective optical potential $V(\mathbf{r}) \propto I(\mathbf{r})/\delta$ for the center-of-mass motion of the atoms, where δ is the detuning between the laser and the atomic transition frequency [22]. We restrict our study to blue-detuned speckles, corresponding

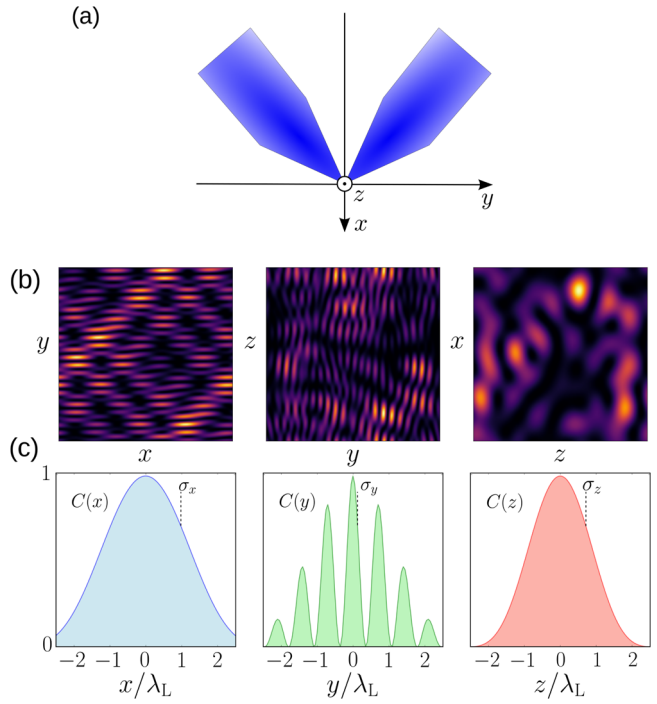

FIG. 1. Properties of the optical disorder potential. (a) Experimental configuration for the generation of an optical disorder potential using two interfering laser beams (along the bisectors of the x and y directions), as used in Refs. [13,14]. (b) A typical numerical realization of the disordered potential in the xy, yz, and zx planes. (c) Numerically computed two-point correlation function of the disordered potential as function of position (in units of the laser wavelength λ_L) along the x, y, and z directions. The three correlation lengths $\sigma_x \approx 0.99$, $\sigma_y \approx 0.13$, and $\sigma_z \approx 0.72$ (see text) are markedly different in such anisotropic experimental configuration, here $\theta_0 = 0.3$.

to $\delta > 0$, which are widely used in experiments. The optical disorder is then always positive and its potential distribution obeys the Rayleigh law. Without loss of generality, it is customary to shift V by its average value V_0, so that the distribution takes the form

$$P(V) = \frac{\Theta(V + V_0)}{V_0} \exp\left(-\frac{V + V_0}{V_0}\right), \tag{1}$$

$\Theta(x)$ being the unit step function. With this choice, $\langle V \rangle = 0$ and $\langle V^2 \rangle = V_0^2$. The fact that the local potential distribution $P(V)$ is not Gaussian and strongly asymmetric—in contrast with model potentials often used in theoretical calculations—has important consequences for the behavior of the mobility edge [23–25].

Optical speckle potentials are spatially correlated. The two-point correlation function

$$\langle V(\mathbf{r}')V(\mathbf{r}' + \mathbf{r})\rangle = V_0^2 C(\mathbf{r}) \tag{2}$$

is characterized by finite correlation lengths, which, as shown below, play a crucial role for the mobility edge. In the simplest model of a three-dimensional isotropic speckle potential (created by a monochromatic laser of wave vector k_L coming from all directions of space), the correlation function is $C(r) = [\sin(r/\sigma)/(r/\sigma)]^2$, where $\sigma = 1/k_L$. For this model potential, the mobility edge has been numerically computed in Ref. [17]: the mobility edge E_c lies *way below* the average potential, $E_c < 0$, a nontrivial behavior confirmed by various approximate theoretical approaches based on the self-consistent theory of localization [19,20].

In the simple case of isotropic correlations in the potential, there is a natural energy scale associated with the correlation length σ, called the correlation energy [18,26]:

$$E_\sigma = \frac{\hbar^2}{m\sigma^2}, \tag{3}$$

where m is the atomic mass. For $V_0 \ll E_\sigma$, the de Broglie wavelength of an atom with energy V_0 is much larger than the correlation length of the potential, so that the particle can tunnel through the disorder barriers. In this so-called "quantum" regime, the mobility edge is expected to be very close to zero. In contrast, for $V_0 \gg E_\sigma$, the matter wave resolves all the details of the disordered potential. In this "classical" regime, the mobility edge is expected to be close to the percolation threshold of the potential, which is very close to $-V_0$ [27]. Among the three characteristic energy scales, E_c, V_0, E_σ, only their ratios matter, so that one has a unique (unknown) scaling function such that

$$\frac{E_c}{V_0} = \mathcal{F}\left(\frac{V_0}{E_\sigma}\right), \tag{4}$$

with $\lim_{x\to 0}\mathcal{F}(x) = 0^-$ and $\lim_{x\to\infty}\mathcal{F}(x) \approx -1$.

The question most relevant to experiments is whether this scaling behavior applies to realistic speckles with *anisotropic* correlation functions. Two different experimental setups have essentially been developed. In Ref. [12], a single diffusive plate was used to create a speckle pattern with a rather strong anisotropy, depending on the numerical aperture θ_0 of the imaging system. For θ_0 small, the correlation lengths parallel and orthogonal to the laser beam (of wavelength λ_L) scale as λ_L/θ_0^2 and λ_L/θ_0, respectively [28]. For experimental setups in which two crossed coherent laser speckles are made to interfere [13,14], additional fringes of spacing $\lambda_L/\sqrt{2}$ appear, as shown in Fig. 1(b). In both cases, different correlation lengths are present in the system, so that it is no longer clear how to define the correlation energy in Eq. (4).

In order to understand the effect of the anisotropy of realistic optical disorder, we have performed quasi-exact numerical calculations for two different speckle geometries and various values of the numerical aperture (details on the numerical procedure can be found in the Supplemental Material [29]). In Fig. 2(a) we plot the normalized mobility

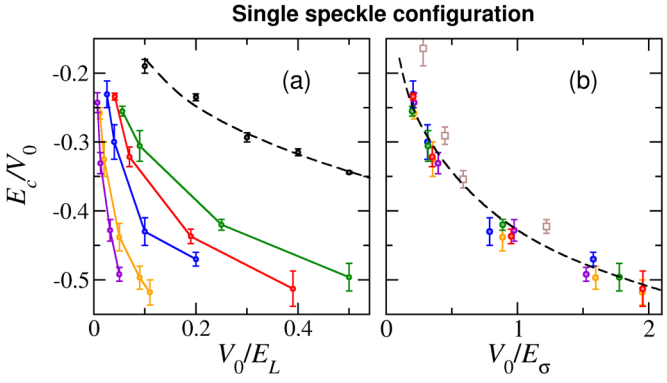

FIG. 2. Mobility edge for atoms in a single laser speckle. (a) Calculated values of the normalized mobility edge E_c/V_0 vs the disorder amplitude V_0 in units of $E_L = \hbar^2 k_L^2/m$ (k_L is the wave vector of the laser beam and m the atomic mass). Different curves correspond to different numerical apertures $\theta_0 = \{0.4, 0.5, 0.7, 0.85, 1.0\}$ (from lower to upper solid colored lines), which control the degree of anisotropy. The black dashed line shows the mobility edge for the isotropic case, obtained by smoothly interpolating the numerical results of Ref. [17] (black symbols). (b) Same data vs the rescaled disorder strength V_0/E_σ, where $E_\sigma = \hbar^2/m(\sigma_\perp^2\sigma_\parallel)^{2/3}$ is the correlation energy. $\sigma_\parallel$ and $\sigma_\perp$ are the correlation lengths along and perpendicularly to the laser beam, respectively, and differ for each θ_0 value. All points approximately lie on the "universal" curve obtained for the isotropic case. Brown squares are the results of an independent estimation of the mobility edge [21], in fair agreement with our results.

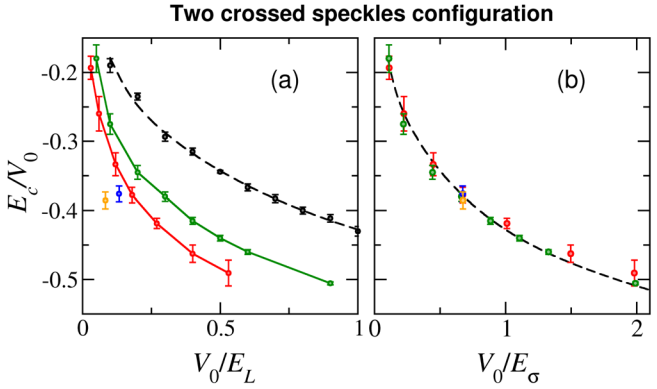

FIG. 3. Normalized mobility edge E_c/V_0 for a two-crossed-speckles configuration [as depicted in Fig. 1(a)] plotted (a) as function of disorder strength V_0 (in units of E_L), (b) as a function of rescaled disorder strength V_0/E_σ with correlation energy $E_\sigma = \hbar^2/m(\sigma_x\sigma_y\sigma_z)^{2/3}$. Values of the numerical aperture are $\theta_0 = \{0.5, 0.8\}$ (respectively, lower and upper solid colored lines) and $\theta_0 = \{0.3, 0.4\}$ (respectively, lower orange and upper blue points). The black dashed line is the same as in Fig. 2. Note that the correlation lengths are modified with respect to the single speckle geometry; see Fig. 1(c).

edge E_c/V_0 for the *single* laser speckle configuration as a function of the disorder amplitude V_0, expressed in units of $E_L = \hbar^2 k_L^2/m$, for five values of the numerical aperture θ_0 controlling the anisotropy. In Fig. 3(a), the same quantity is plotted for a disordered potential generated by *two* crossed coherent laser speckles, for four values of θ_0. The first striking observation is that the mobility edge is always negative (i.e., below the average potential) for all anisotropic configurations, as for the isotropic speckle whose results are also plotted in the figures. The second striking observation is that, although the mobility edge values widely depend on the anisotropy, the behavior in each case is strongly similar.

This suggests that the scaling law, Eq. (4), can be extended to the anisotropic case by an appropriate redefinition of the correlation energy. For anisotropic disorder, it is customary [12,14] to define the correlation energy using the geometric average of the correlation lengths along the three directions (see the justification in the Supplemental Material [29]), namely,

$$E_\sigma = \frac{\hbar^2}{m(\sigma_x\sigma_y\sigma_z)^{2/3}}, \tag{5}$$

with σ_x, σ_y, and σ_z being the correlation lengths of the disorder along the major axes. These are defined here as the half-width at half-maximum of the central correlation peak divided by the numerical factor $\gamma \approx 1.39156$ (such that $\sin\gamma/\gamma = 1/\sqrt{2}$); see Fig. 1(c). This ensures the compatibility with the definition used in Ref. [17] for the isotropic case. Since the correlation lengths along the three axes are larger in the isotropic case [see Fig. 1(c)], the anisotropic speckle scatters less efficiently the atoms, resulting in a larger mean free path ℓ at the same disorder strength and energy. The mobility edge, which is roughly determined by the Ioffe-Regel criterion $k\ell \approx 1$, then occurs at a lower momentum k, that is at lower energy. This qualitatively explains why in Figs. 2(a)–3(a) all curves are shifted downwards as θ_0 decreases.

In Figs. 2(b) and 3(b), we replot the same numerical values of the mobility edge vs the rescaled disorder strength V_0/E_σ for the various anisotropic configurations, each configuration having a specific $E_\sigma(\theta_0)$ horizontal rescaling factor as defined in Eq. (5). Amazingly, all curves collapse on a *single* universal curve, independently of the anisotropy and whether the speckle pattern is created by a single laser beam or two crossed beams. This constitutes a major result of this Letter, as it allows us to take into account all complications introduced by the inherent anisotropy of experimental speckle disorder through a simple rescaling of the characteristic energies.

Strictly speaking, this universality cannot be exact, as details of the disorder correlation function must have an influence on the position of the mobility edge. However, the system being strongly scattering at the mobility edge (according to the Ioffe-Regel criterion, the mean free-path is shorter than the de Broglie wavelength), long-range correlations in the potential are essentially irrelevant. This universality is more accurate in the quantum regime

$V_0 \ll E_\sigma$ where the matter wave averages out the disordered potential. In the regime of current cold-atom experiments, the universal function $\mathcal{F}$ allows us to predict the position of the mobility edge within a few percent, which is largely enough considering that the discrepancy between experimental results and theoretical predictions is of the order of 100% or higher.

Recently, the position of the mobility edge in the single speckle configuration has been estimated in Ref. [21], using a different method based on the statistical properties of the energy spectrum. We have added the corresponding points—which lie slightly above our results—in Fig. 2(b).

To date, three different cold-atom experiments have reported measurements of the mobility edge in blue-detuned speckle disorder [12–14]. Although these experiments do not use the same setup for the generation of the optical disorder potential and hence have different potential correlation functions, they share the same technique to probe the mobility edge: prepare a wave packet localized in configuration space and let it expand in the presence of disorder. In the experiments, the energy distribution of the wave packet—which should be as narrow as possible—may extend on the two sides of the mobility edge, yielding a localized fraction of atoms at long times. By measuring this quantity and knowing the energy distribution of the initial wave packet, one can infer the position of the mobility edge. The three experiments use different techniques to determine the localized fraction and the energy distribution, each having its advantages and drawbacks.

The universal scaling of the mobility edge predicted above allows a direct quantitative comparison of our numerical results with the available experimental data, which are gathered in Fig. 4. The experiment of Ref. [12] used a very anisotropic single speckle configuration. The use of spin-polarized fermionic atoms allowed the authors of Ref. [12] to avoid atom-atom interactions and to have a rather well-known energy distribution in the absence of disorder. However, the disorder strength used in this experiment is large and surely affects the energy distribution. Moreover, the duration of the experiment may have been too short to detect slow diffusion above the mobility edge [36], leading to an overestimation of the lowest diffusive energy. As can be seen in the inset of Fig. 4, their inferred mobility edge is large and positive (that is above the average potential), in contradiction with all numerical and theoretical predictions. We thus conclude that these results are impaired by some severe imperfections.

The experiment of Ref. [13] used two crossed speckles to achieve a more isotropic configuration. The wave packet is prepared with a narrow energy distribution in the *absence* of disorder; the disorder being applied abruptly, the energy distribution of the atoms in the *presence* of disorder is much broader—extending on both sides of the mobility edge—resulting in a rather small localized fraction. An estimate of the mobility edge (see Ref. [13] for detailed explanations

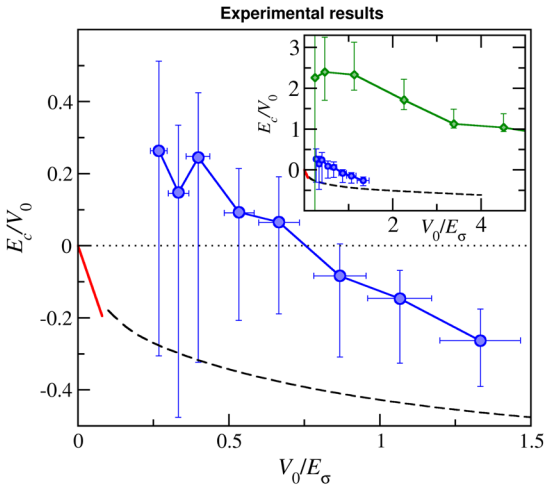

FIG. 4. Experimental values of the mobility edge for non-interacting cold atoms in blue-detuned speckle disorder inferred from three different experiments. Both Ref. [13] (red line, in the weak disorder regime) and Ref. [14] (blue line, with error bars) use two crossed coherent speckles, while the setup of Ref. [12] uses a single, strongly anisotropic, speckle (green line in the inset, with error bars). The correlation energy E_σ has been computed using the correlation lengths provided in each article. The universal curve for the mobility edge—extracted from previous [17] numerical results for isotropic speckles and validated for anisotropic speckles in Figs. 2–3—is also represented for reference (black dashed line). The horizontal dotted line is the average potential.

on the procedure used) yields the straight red line $E_c/V_0 = -2.44 V_0/E_\sigma$ shown in Fig. 4, in fair agreement with our numerical predictions and notably below the average potential.

The most recent experiment of Ref. [14] used a similar two-speckles configuration. Thanks to the control of atom-atom interactions via a Feshbach resonance, it was possible to prepare a rather narrow energy distribution in the presence of the disorder. When the disorder amplitude is rescaled by the appropriate E_σ, the qualitative behavior of the inferred mobility edge versus V_0 is similar to our numerical results, but quantitatively too high. The origin of this deviation is not entirely clear to us at the moment.

To summarize, we computed numerically the mobility edge for noninteracting cold atoms in three-dimensional speckle potentials, taking into account the long-range anisotropic disorder correlations that characterize realistic experimental configurations. We have shown that the mobility edge displays a robust scaling property when the anisotropy of the speckle geometry is varied, the correlation energy of the potential—defined from the geometric mean of the correlation lengths—being the scaling parameter. While the early experimental results in Ref. [13] seem in fair agreement with our predictions, we observe strong discrepancies with Ref. [12]. The more accurate measurements reported in Ref. [14] are closer to

our quasi-exact numerical simulations, but still show significant deviations, calling for further studies. The nontrivial scaling law for the position of the mobility edge unveiled in this Letter provides strong guidance for the next generation of such experiments striving to measure the critical exponents and multifractal behavior appearing right at the transition point.

We acknowledge discussions with V. Josse and thank S. Pilati for sending us the raw data of Ref. [21]. M. P. was supported by ERC (Advanced Grant "Quantatop") and the Region Ile-de-France in the framework of DIM Nano-K (project QUGASP). The authors were granted access to the HPC resources of TGCC under the allocations 2014-057301, 2015-057301, 2015-057083, 2016-057629, and 2016-057644 made by GENCI ("Grand Equipement National de Calcul Intensif").

*michael.pasek@lkb.upmc.fr
Present address: Collège de France, 11 place Marcelin Berthelot, 75005 Paris, France.

[1] P. W. Anderson, Absence of diffusion in certain random lattices, Phys. Rev. **109**, 1492 (1958).
[2] D. S. Wiersma, P. Bartolini, A. Lagendijk, and R. Righini, Localization of light in a disordered medium, Nature (London) **390**, 671 (1997).
[3] M. Störzer, P. Gross, C. M. Aegerter, and G. Maret, Observation of the critical regime near Anderson localization of light, Phys. Rev. Lett. **96**, 063904 (2006).
[4] T. Schwartz, G. Bartal, S. Fishman, and M. Segev, Transport and Anderson localization in disordered two-dimensional photonic lattices, Nature (London) **446**, 52 (2007).
[5] Y. Lahini, A. Avidan, F. Pozzi, M. Sorel, R. Morandotti, D. N. Christodoulides, and Y. Silberberg, Anderson Localization and Nonlinearity in One-Dimensional Disordered Photonic Lattices, Phys. Rev. Lett. **100**, 013906 (2008).
[6] H. Hu, A. Strybulevych, J. H. Page, S. E. Skipetrov, and B. van Tiggelen, Localization of ultrasound in a three-dimensional elastic network, Nat. Phys. **4**, 945 (2008).
[7] A. A. Chabanov, M. Stoytchev, and A. Z. Genack, Statistical signatures of photon localization, Nature (London) **404**, 850 (2000).
[8] J. Billy, V. Josse, Z. Zuo, A. Bernard, B. Hambrecht, P. Lugan, D. Clément, L. Sanchez-Palencia, P. Bouyer, and A. Aspect, Direct observation of Anderson localization of matter waves in a controlled disorder, Nature (London) **453**, 891 (2008).
[9] G. Roati, C. d'Errico, L. Fallani, M. Fattori, C. Fort, M. Zaccanti, G. Modugno, M. Modugno, and M. Inguscio, Anderson localization of a non-interacting Bose-Einstein condensate, Nature (London) **453**, 895 (2008).
[10] S. Katsumoto, F. Komori, N. Sano, and S. Kobayashi, Fine tuning of metal-insulator transition in $Al_{0.3}Ga_{0.7}As$ using persistent photoconductivity, J. Phys. Soc. Jpn. **56**, 2259 (1987).
[11] S. Waffenschmidt, C. Pfleiderer, and H. v. Löhneysen, Critical Behavior of the Conductivity of Si:P at the Metal-Insulator Transition under Uniaxial Stress, Phys. Rev. Lett. **83**, 3005 (1999).
[12] S. S. Kondov, W. R. McGehee, J. J. Zirbel, and B. DeMarco, Three-dimensional Anderson localization of ultracold matter, Science **334**, 66 (2011).
[13] F. Jendrzejewski, A. Bernard, K. Muller, P. Cheinet, V. Josse, M. Piraud, L. Pezzé, L. Sanchez-Palencia, A. Aspect, and P. Bouyer, Three-dimensional localization of ultracold atoms in an optical disordered potential, Nat. Phys. **8**, 398 (2012).
[14] G. Semeghini, M. Landini, P. Castilho, S. Roy, G. Spagnolli, A. Trenkwalder, M. Fattori, M. Inguscio, and G. Modugno, Measurement of the mobility edge for 3D Anderson localization, Nat. Phys. **11**, 554 (2015).
[15] F. Evers and A. D. Mirlin, Anderson transitions, Rev. Mod. Phys. **80**, 1355 (2008).
[16] C. A. Müller, D. Delande, and B. Shapiro, Critical dynamics at the Anderson localization mobility edge, Phys. Rev. A **94**, 033615 (2016).
[17] D. Delande and G. Orso, Mobility edge for cold atoms in laser speckle potentials, Phys. Rev. Lett. **113**, 060601 (2014).
[18] R. C. Kuhn, O. Sigwarth, C. Miniatura, D. Delande, and C. A. Müller, Coherent matter wave transport in speckle potentials, New J. Phys. **9**, 161 (2007).
[19] M. Piraud, L. Sanchez-Palencia, and B. van Tiggelen, Anderson localization of matter waves in three-dimensional anisotropic disordered potentials, Phys. Rev. A **90**, 063639 (2014).
[20] A. Yedjour and B. van Tiggelen, Diffusion and localization of cold atoms in 3D optical speckle, Eur. Phys. J. D **59**, 249 (2010).
[21] E. Fratini and S. Pilati, Anderson localization of matter waves in quantum-chaos theory, Phys. Rev. A **91**, 061601 (2015).
[22] C. Cohen-Tannoudji, J. Dupont-Roc, and G. Grynberg, *Atom-Photon Interactions: Basic Processes and Applications* (Wiley, New York, 1992).
[23] D. Semmler, J. Wernsdorfer, U. Bissbort, K. Byczuk, and W. Hofstetter, Localization of correlated fermions in optical lattices with speckle disorder, Phys. Rev. B **82**, 235115 (2010).
[24] M. Pasek, Z. Zhao, D. Delande, and G. Orso, Phase diagram of the three-dimensional Anderson model for short-range speckle potentials, Phys. Rev. A **92**, 053618 (2015).
[25] E. Fratini and S. Pilati, Anderson localization in optical lattices with correlated disorder, Phys. Rev. A **92**, 063621 (2015).
[26] R. C. Kuhn, C. Miniatura, D. Delande, O. Sigwarth, and C. A. Müller, Localization of matter waves in two-dimensional disordered optical potentials, Phys. Rev. Lett. **95**, 250403 (2005).
[27] S. Pilati, S. Giorgini, M. Modugno, and N. Prokof'ev, Dilute Bose gas with correlated disorder: A path integral Monte Carlo study, New J. Phys. **12**, 073003 (2010).
[28] J. Goodman, *Speckle Phenomena in Optics: Theory and Applications* (Dover, New York, 2007).

[29] See Supplemental Material at http://link.aps.org/supplemental/10.1103/PhysRevLett.118.170403, which includes Refs. [30–35], for details on the numerical procedure and rationale behind the definition of correlation energy in anisotropic correlated disorder.
[30] M. Piraud, Ph. D. thesis, Université Paris Sud-Paris XI, 2012.
[31] M. Piraud, L. Pezzé, and L. Sanchez-Palencia, Quantum transport of atomic matter waves in anisotropic two-dimensional and three-dimensional disorder, New J. Phys. **15**, 075007 (2013).
[32] A. McKinnon and B. Kramer, The scaling theory of electrons in disordered solids: additional numerical results, Z. Phys. B **53**, 1 (1983).
[33] P. Wölfle and R. N. Bhatt, Electron localization in anisotropic systems, Phys. Rev. B **30**, 3542 (1984).
[34] M. Piraud, L. Pezzé, and L. Sanchez-Palencia, Matter wave transport and Anderson localization in anisotropic three-dimensional disorder, Europhys. Lett. **99**, 50003 (2012).
[35] R. N. Bhatt, P. Wölfle, and T. V. Ramakrishnan, Localization and interaction effects in anisotropic disordered electronic systems, Phys. Rev. B **32**, 569 (1985).
[36] C. A. Müller and B. Shapiro, Comment on Three-Dimensional Anderson Localization in Variable Scale Disorder, Phys. Rev. Lett. **113**, 099601 (2014).